JAIST Robotic Walker Control Based on a Two-layered Kalman Filter

Geunho Lee, Eui-Jung Jung, Takanori Ohnuma, Nak Young Chong, and Byung-Ju Yi

***Abstract*— This paper presents a new control scheme of JAIST Active Robotic Walker (JARoW) developed to provide elderly people with sufficient ambulatory capability. Toward its practical use, our focus is placed on how to allow easier and reliable maneuverability by creating a natural user interface. Specifically, our challenge lies in providing a well-functioning controller by detecting what the user wants to do or their intentions. A Kalman filter based tracking scheme is realized to estimate and predict the locations of the user's legs and body in real time. The feedback control can then adjust the motions of JARoW corresponding to the actual user's walking behaviors. Our experiments confirm that JARoW can autonomously adjust its motion direction and velocity without requiring any additional control inputs.**

I. INTRODUCTION

Personal mobility aids are strongly desired to help elderly and/or lower limb disabled people stay independent. Recent advances in robot technology have provided a solid foundation for the development of various walking aids. Notable examples include wheelchairs [1][2], canes [3], and walkers [4]-[7]. Depending on different levels of ambulatory capability, robotic wheelchairs [1][2] are one of the most widely used mobility aids. Unanticipated problems reported include muscle weakness due to long-time sitting or mental stress from the lower line-of-sight. Robotic walkers can be further divided into passive [4][5] and active walkers [6][7]. The features of passive walkers include low cost, simple structure, and compact size. However, users must take overly cautious steps not to push it out too far forward. Also, it is deemed to be unsafe to use on uneven/slope terrain. Active walkers may provide both ambulatory aid and rehabilitation. However, they are still bulky and costly, and their complicated operation often requires considerable skill to use. Toward more widespread use of active walkers, there are many things that need to be taken into consideration. For instance, elderly people are slow in behavior and not familiar with mechanical or electronic controls. Therefore, a simple and natural user interface is of particular importance. To meet these requirements, voice activation systems have been presented in [8]. Despite their many advantages, there are critical problems such as interference and recognition that remain to be resolved. Instead of using the user's command directly, it would be very convenient if his/her intention can be recognized by robotic walkers. A few examples include the visual recognition using cameras [9] and human gait detection based on pressure sensors [10]. However, under real world conditions, it is difficult to guarantee their reliability.

G. Lee, T. Ohnuma, and N.Y. Chong are with the School of Information Science, Japan Advanced Institute of Science and Technology, Ishikawa, Japan {geun-lee, t-ohnuma, nakyoung}@jaist.ac.jp

E.-J. Jung and B.-J. Yi are with the School of Electrical Engineering and Computer Science, Hanyang University, Ansan, Korea

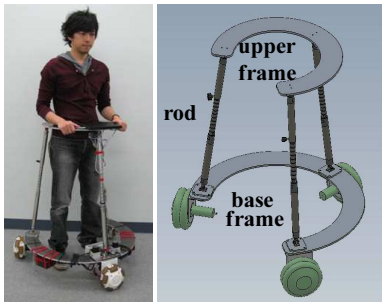

Fig. 1. JAIST active robotic walker (JARoW) prototype

We developed the first JARoW prototype in 2009 [11] which offers a basic navigation capability (see Fig. 1). The main objective of this paper is to present an enhanced navigation control method for JARoW, enabling to provide elderly people with sufficient ambulatory capability in all directions achieved by natural, unconstrained, and omni-directional walking. There is always a challenge on how to design a natural interface and a feedback control in the presence of sensor measurement faults. For the purpose, a Kalman filter based tracking scheme is realized to estimate and predict the locations of the user's lower limbs and body in real time. The feedback control can then adjust the motions of JARoW corresponding to the user's walking behaviors. Moreover, the obstacle avoidance scheme employing the potential field technique is implemented to move safely and smoothly in the indoor environment. We describe the proposed control algorithms in detail, and perform extensive experiments to demonstrate their effectiveness in our laboratory environment.

II. JAROW: SYSTEM DESCRIPTION

A. Control Architecture

JARoW autonomously adjusts its direction and displacement according to the user's walking behavior without requiring any additional user effort. Specifically, JARoW consists of the drive-train, the interface system, and the main controller. We use a laptop PC that runs on Microsoft's Windows XP as the main controller. The input to the main controller includes the measurement data obtained from the interface system. Based on the data, a Kalman filter based tracking scheme estimates and predicts the locations of the user's lower limbs and body with respect to JARoW's local coordinates. The feedback motion control scheme then outputs the desired velocity matrix to the drive-train at each

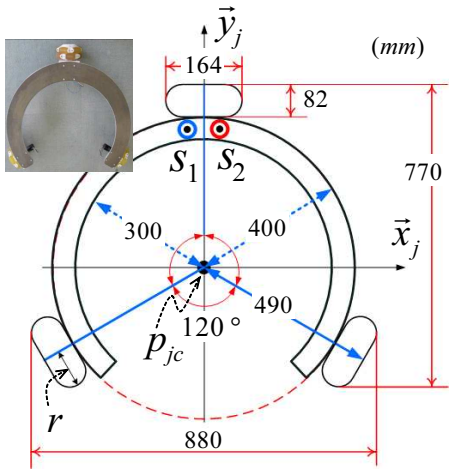

Fig. 2. Specification and notations of the base frame

time step. Details on the control scheme will be explained in the following sections.

B. Mechanical Structure and Hardware Configuration

A compact design, such as 825 $\sim$ 1000 *mm* in height, and 880 *mm* and 770 *mm* in horizontal diameters, saves cost and uses less space. It is therefore considered to be suited for use in various environments including narrow hallways or elevators. As shown in Fig. 1, the outline is a circular shape to reduce possible collisions with obstacles or walls. Its stiff and light design of 20 *kg* is achieved with an aluminum alloy.

JARoW has three main structural parts: base frame, upper frame, and connecting rods. The base frame is to support the superstructure, and is directly connected to three omni-directional wheels and equipped with a pair of Hokuyo URG-04LX laser range finders (LRFs) detecting the user's lower limb locations. The length of the connecting rod can be changed up to 175 *mm* according to the height of users. Users are able to lean their upper body forward and place their forearm onto the upper frame. The main controller is mounted on top of the upper frame.

The drive-train is composed of three Mecanum wheels, three motors equipped with encoder and 43:1 gear reduction unit, three motor drivers, and one motor controller. Three Mecanum wheels are mounted underneath the base frame 120 degrees apart from each other (see Fig. 2), allowing JARoW to move forward/backward, slide sideways, and turn right/left. Such omni-directionality provides an efficient means of direction control in highly cluttered indoor environments. The maximum stall torque is determined in such a way that JARoW can accommodate up to 90 *kg*. It is reported that the average maximum walking speed for elderly pedestrians is 4.8 km/h on flat terrain [12]. The maximum continuous torque is determined to meet the maximum velocity requirement 6.58 km/h of the drive-train.

C. Interface System

As shown in Fig. 3, a pair of LRFs detects the locations of the user's lower limbs, as well as obstacles or area borders.

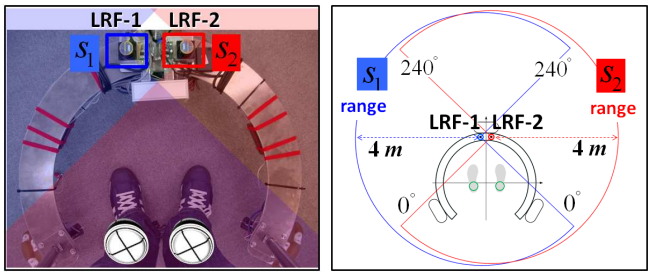

(a) cylinder-like model (b) coverage area of LRF

Fig. 3. Lower limbs modeled as a cylinder with a diameter d

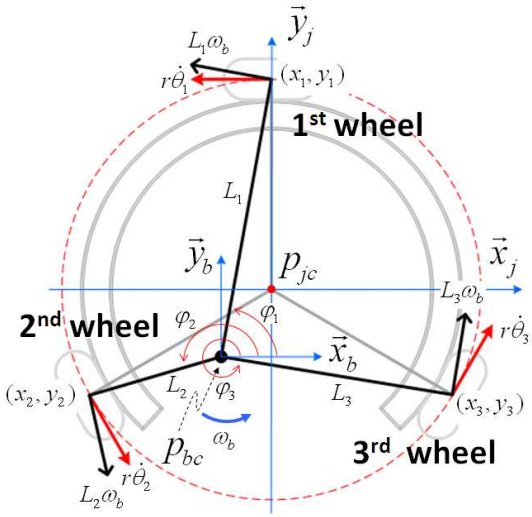

Fig. 4. Illustration of JARoW kinematics

The lower limbs are modeled as a cylinder with a diameter d, representing each shin as illustrated in Fig. 3-(a). Further details on this model can be found in [11]. We define a valid region for the location measurement of shins as a rectangle with 900 $\times$ 700 *mm* (length and width) inside the base frame. It is assumed that the locations of shins always remain within its region.

Each LRF outputs a 240 degree scan and measures up to 4000 *mm* with 100 *ms* sampling time. Accordingly, a pair of LRFs can cover a full 360 degrees. After each scan, the range data from the individual LRF rays are sorted into surface information of shins and obstacles, respectively, according to pre-determined regions. The interface system outputs the LRF-to-surface distance that is fed to the main controller.

D. Kinematics

As shown in Fig. 2, JARoW has its local coordinates $\vec{x}_j$ (vertical axis) and $\vec{y}_j$ (horizontal axis). Its center position is denoted as p_{jc}. S_1 and S_2 denote the positions of LRFs. For a mobile robot with Mecanum wheels, the *Instantaneous Center of Rotation* (ICR) corresponds to its centroid during rotation. In contrast, we set the ICR to the center of the user body defined as $p_{bc} = (x_b, y_b)$ in Fig. 4, the midpoint of the line segment connecting the center points of two circles projecting both shins onto the ground. By doing this, JARoW effectively avoids being bumped into the user while it rotates.

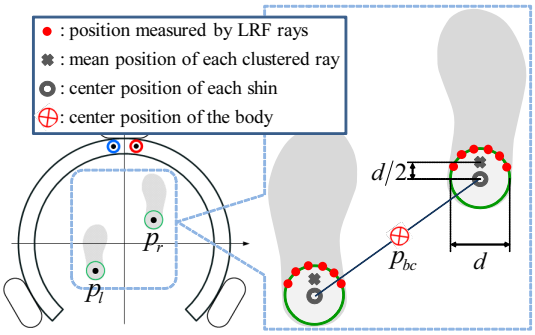

Fig. 5. Definitions and notations used in the formulation

Now, the first-order kinematics of JARoW can be derived. $\dot{\theta}_i$ and φ_i denote the driving angular velocity of the *i*-th wheel and the angular displacement of the *i*-th wheel relative to $\vec{x}_b$-axis in the user body reference frame $\vec{x}_b$ and $\vec{y}_b$, respectively. Using the tangent formula, φ_i is computed:

$$\varphi_i = \tan^{-1}(\frac{y_i - y_b}{x_i - x_b}). \tag{1}$$

Next, L_i which denotes the distance between p_{bc} and each wheel position (x_i, y_i) is given by

$$L_i = \sqrt{(y_i - y_b)^2 + (x_i - x_b)^2}. \tag{2}$$

For the desired JARoW velocity vector $[\dot{x}_b \ \dot{y}_b \ \omega_b]^t$, the angular velocities $\dot{\theta}_1$, $\dot{\theta}_2$, and $\dot{\theta}_3$ of individual wheels through the inverse Jacobian are derived:

$$\begin{bmatrix} \dot{\theta}_1 \\ \dot{\theta}_2 \\ \dot{\theta}_3 \end{bmatrix} = \frac{1}{r} \begin{bmatrix} -1 & 0 & L_1 \cos(\frac{\pi}{2} - \varphi_1) \\ \cos\frac{\pi}{3} & -\sin\frac{\pi}{3} & L_2 \cos(\frac{7\pi}{6} - \varphi_2) \\ \cos\frac{\pi}{3} & \sin\frac{\pi}{3} & L_3 \cos(\frac{\pi}{6} + \varphi_3) \end{bmatrix} \begin{bmatrix} \dot{x}_b \\ \dot{y}_b \\ \omega_b \end{bmatrix}, \tag{3}$$

where r denotes the wheel radius.

III. Interface Functions

A. Kalman Filter Based Tracking

The Kalman filtering [13] is utilized to measure the locations of shins accurately against the possibility of sensor measurement faults. In practice, the shin locations remain uncertain. For example, two legs frequently occlude each other. In order to robustly estimate the shin locations p_r and p_l, a two layered Kalman filter for p_r, p_l, and p_{bc} is proposed.

Measurement data for the surface of shins are represented as red circles in Fig. 5. After each sampling time, they are divided into left and right clusters, and then the mean positions of these clusters are calculated. Through preliminary tests by 10 people, we empirically learned that the mean positions were in the immediate vicinity of the cylinder's surface and the distances from the mean position to p_r or p_l were approximately one-half of its diameter d. Therefore, $p_l = (x_l, y_l)$ and $p_r = (x_r, y_r)$ can be obtained by adding the mean position to $d/2$.

To track the user's walking movement continuously in the presence of uncertainties, a data association technique [14] is employed, matching current shin location candidates to previous shin locations after each sampling time T. In other words, validated measurements nearest to the prediction values are used for updating in the next state. The state vector $\mathbf{x}_{i,k}$ representing the position and velocity of p_r or p_l with respect to $\vec{x}_j$ and $\vec{y}_j$ is defined:

$$\mathbf{x}_{i,k} = [x_{i,k} \ y_{i,k} \ \dot{x}_{i,k} \ \dot{y}_{i,k}]^t, \tag{4}$$

where i denote the left or right side. It is assumed that each shin moves with constant velocity. By the Kalman filter model, the state transition from k to $k+1$ is described:

$$\mathbf{x}_{i,k+1} = \mathbf{F}_{i,k}\mathbf{x}_{i,k} + w_k, \tag{5}$$

where $\mathbf{F}_{i,k}$ is the state transition matrix given by

$$\mathbf{F}_{i,k} = \begin{bmatrix} \mathbf{I} & T\mathbf{I} \\ \mathbf{0} & \mathbf{I} \end{bmatrix}. \tag{6}$$

and w_k means the system noise which is assumed to be zero mean Gaussian white noise with covariance Q_k, $w_k \sim N(0, Q_k)$. Additionally, T indicates the sampling time interval 100 ms. The predicted estimate covariance can be obtained:

$$\mathbf{P}_{i,k+1|k} = \mathbf{F}_{i,k} \ \mathbf{P}_{i,k|k} \ \mathbf{F}_{i,k}^t + Q_k, \tag{7}$$

where Q_k is given by

$$Q_k = \sigma_c^2 \begin{bmatrix} T^4/4 & T^3/2 \\ T^3/2 & T^2 \end{bmatrix} \mathbf{I}. \tag{8}$$

Next, the measurement equation is formalized:

$$\mathbf{z}_{i,k} = \mathbf{H}_{i,k}\mathbf{x}_{i,k} + v_k, \tag{9}$$

where the observation relation function matrix $\mathbf{H}_k$ is given by

$$\mathbf{H}_{i,k} = \begin{bmatrix} \mathbf{I} & \mathbf{0} \end{bmatrix}, \tag{10}$$

and v_k is the measurement random noise which is assumed to be zero mean Gaussian white noise with covariance R_k, $v_k \sim N(0, R_k)$. Moreover, the noises w_k and and v_k at k are all assumed to be mutually independent. The innovation covariance by the measurement sensor error is given by

$$\mathbf{S}_{i,k} = \mathbf{H}_{i,k} \ \mathbf{P}_{i,k|k-1} \ \mathbf{H}_{i,k}^T + R_k, \tag{11}$$

where R_k is the covariance of the relative state measurements. Thus, the filtered state estimate and the error covariance are obtained:

$$\begin{array}{lcl} \mathbf{K}_{i,k+1} & = & \mathbf{P}_{i,k+1|k} \ \mathbf{H}_{i,k+1}^t \ \mathbf{S}_{i,k+1}^{-1} \\ \hat{\mathbf{x}}_{i,k+1|k+1} & = & \hat{\mathbf{x}}_{i,k+1|k} + \mathbf{K}_{i,k+1} \ \tilde{\mathbf{z}}_{i,k+1} \\ \mathbf{P}_{i,k+1|k+1} & = & \mathbf{P}_{i,k+1|k} - \mathbf{K}_{i,k+1} \ \mathbf{S}_{i,k+1} \ \mathbf{K}_{i,k+1}^t \end{array}, \tag{12}$$

where $\mathbf{K}_{i,k+1}$, $\hat{\mathbf{x}}_{i,k+1|k+1}$, and $\mathbf{P}_{i,k+1|k+1}$ are a Kalman gain, an updated state estimate, and an updated estimate covariance, respectively.

Based on the estimated p_r and p_l, the p_{bc} candidate is defined as the midpoint on the line segment connecting these estimates as illustrated in Fig. 5. Specifically, p_{bc} is considered to be the body position. The motion of p_{bc} is also assumed to be at constant velocity. Then, the filtering formulations from (4) to (12) can also be utilized for the body matching. When one shin data is not available at any sampling time, the interface system can still estimate p_{bc} due to the proposed two-layered Kalman filter.

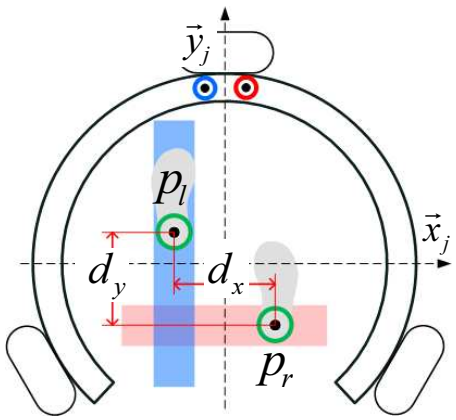

Fig. 6. Definitions and notations of the distances d_x and d_y between p_r and p_l in $\vec{x}_j$ and $\vec{y}_j$ directions during moving forward

B. Area Detection

Based on the distance-to-surface data for obstacles and/or area borders, one of the well-known obstacle avoidance algorithms, the potential field technique [15], is utilized. According to the distance data, the potential field is generated:

$$PF(d_o) = \begin{cases} 0 & (d_o \geq d_{max}) \\ \frac{(d_o - d_{max})^2}{(d_{min} - d_{max})^2} & (d_{min} < d_o < d_{max}) \\ 1 & (d_{min} \geq d_o) \end{cases}, \quad (13)$$

where d_o, d_{min}, and d_{max} denote the distance from p_{jc} to the border of an obstacle, a minimum permissible distance, and a maximum influence distance. The generated potential field is transmitted to the motion control function.

IV. Motion Control Functions

A. Feedback Motion Control

The basic idea behind the proposed control is that p_{jc} and p_{bc} must remain coincident with each other. For this, a *Proportional-plus-Integral-plus-Derivative* (PID) controller is implemented. Based on the PID control technique, preliminary tests for walking behaviors of 10 people were performed and analyzed. From these results, typical behavior patterns of moving forward/backward and turning right/left are modeled.

1) PID controller: Separating the center position errors e_x and e_y of p_{bc} according to $\vec{x}_b$ and $\vec{y}_b$ directions with respect to $\vec{x}_j$ and $\vec{y}_j$, e_x and e_y are defined as $e_x = x_j - x_b$ and $e_y = y_j - y_b$ that need to be minimized:

$$\begin{cases} \dot{x}_b &= K_{p,x}\, e_x + K_{i,x} \int e_x dt + K_{d,x}\, \dot{e}_x \\ \dot{y}_b &= K_{p,y}\, e_y + K_{i,y} \int e_y dt + K_{d,y}\, \dot{e}_y \end{cases}, \quad (14)$$

where $\dot{x}_b$ and $\dot{y}_b$ are input velocities of JARoW in (3), and K_p, K_i, and K_d denote the proportional, integral, and derivative gains, respectively.

Preliminary tests for walking behaviors of 10 people were performed for 20 seconds after applying the Kalman filtered tracking and PID control techniques. We then analyze the distance between p_r and p_l in the $\vec{x}_j$ direction, denoted by d_x in Fig. 6. TABLE I shows the mean and standard deviation of the estimated d_x that does not significantly change.

TABLE I

STATISTICAL ANALYSIS OF THE ESTIMATED d_x DISTANCE DATA (mm)

person	A	B	C	D	E	F
mean	178.85	167.99	159.17	139.68	133.48	129.32
SD	18.01	15.59	13.45	15.57	9.87	10.64
person	G	H	I	J	average	SD
mean	167.28	176.95	183.63	132.23	156.86	20.12
SD	16.02	11.60	18.29	13.93	14.30	2.78

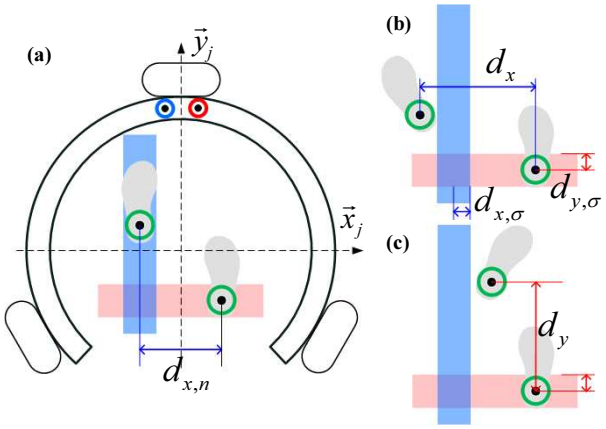

Fig. 7. Definitions and notations used in (a) moving forward, (b) turning left, (c) turning right

2) Rotation motion control: In contrast to the results presented in TABLE I, there appears to be a wide variation in d_x when turning right/left according to the direction of rotation. In Fig. 7, $d_{x,n}$ indicates the mean distance between p_r and p_l during moving forward/backward, and $d_{x,\sigma}$ and $d_{y,\sigma}$ denote the boundaries of distance variations which are determined by referring the standard deviation of the distances, respectively. Employing these parameters, walking behaviors are classified into three patterns:

$$\begin{cases} d_{x,n} + d_{x,\sigma} \geq d_x & \text{(turning left)} \\ d_{x,n} - d_{x,\sigma} < d_x < d_{x,n} + d_{x,\sigma} & \text{(moving forward)} \\ d_{x,n} - d_{x,\sigma} \geq d_x & \text{(turning right)} \end{cases}. \quad (15)$$

Depending on individuals, the moving forward/backward behavior shows different variations in d_x. For the purpose, the distance boundary d_y in the $\vec{y}_j$ direction as illustrated in Fig. 7-(c) is limited to a distance smaller than $2 \times d_{y,\sigma}$.

Fig. 8 illustrates the concept for the rotation motion control. As the turning right/left behavior is detected, the motion control outputs a pre-determined velocity matrix to each motor of the drive-train until d_x is satisfied within the designed range. As mentioned in (3), JARoW rotates on the axis of p_{bc} in the direction where any shin is ahead of the other with respect to $\vec{x}_j$ and $\vec{y}_j$ (see Fig. 8-(a)).

B. Obstacle Avoidance

When the potential field (13) is utilized, JARoW will stop as soon as it detects an obstacle/border, which makes users very uncomfortable and possibly bump into the upper frame. Therefore, the potential field is modified to enable JARoW

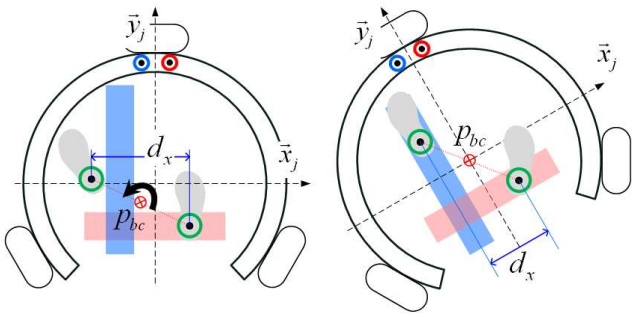

(a) before turning left (b) after turning left

Fig. 8. Illustration of the turning left motion

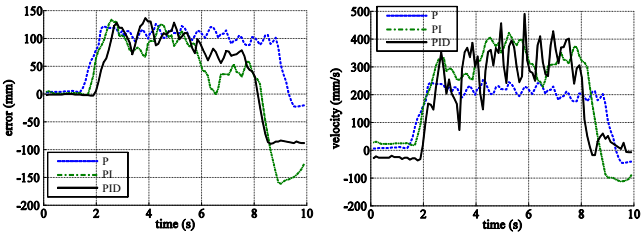

(a) position errors (b) velocities of the JARoW

Fig. 9. Three types of feedback control for moving forward behavior

to naturally reduce its speed according to the distances to obstacles. The overall motion control function is defined below describing how JARoW uses the potential field:

$$\begin{cases} \dot{x}_{out} &= \dot{x}_b(1 - PF(d_o)) \\ \dot{y}_{out} &= \dot{y}_b(1 - PF(d_o)) \end{cases} . \quad (16)$$

V. Experimental Results and Discussion

This section presents the test results of an enhanced control capability of JARoW. It moves with the maximum linear velocity of 4.8 *km/h*. When it makes rotational motion, the magnitude of the angular velocity is 0.5 rad/s and the direction of the angular velocity is decided by (15), where $d_{x,\sigma}$ and $d_{y,\sigma}$ are empirically set to 2.78 and 7.9 mm, respectively. In (13), d_{min} and d_{max} are pre-determined as 500 and 2500 mm, respectively.

First, to examine the performances of JARoW's feedback motion corresponding to the user's moving forward behavior, individual motion controls only employing P, PI, and PID controllers, respectively, were tested for 10 seconds. The gains of each controller are set to $K_{p,y}$ = $K_{p,x}$ =2, $K_{i,y}$ = $K_{d,y}$ =0.5, and $K_{i,x}$ = $K_{d,x}$ =0.2, respectively. In these experiments, the user started walking at 2 seconds and stops around 9 seconds. Fig. 9 presents the comparison results for e_y and $\dot{y}_b$ in the $\vec{y}_j$ direction. Here, the blue dotted line, green dash-dotted line, and black solid line indicate the results with P, PI, and PID control, respectively. The P-only controller could not pick up the user velocities exceeding 300 mm/s. When the PI controller was employed, an overshoot arises as the user velocities change. The PID controller showed excellent performance within about 100 *mm* errors. The results demonstrate that JARoW could control its forward motion

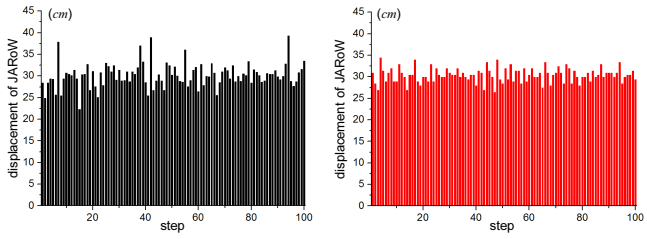

(a) previous motion control [11] (b) proposed motion control

Fig. 10. JARoW displacements according to user's stride lengths

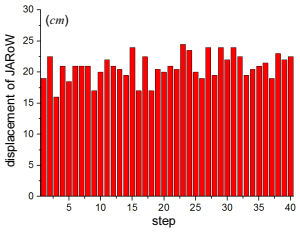

(a)

	step right	step left
mean	20.86	21.23
SD	2.10	2.24
min	16.0	17.0
max	24.5	26.0

(b)

Fig. 11. JARoW displacement according to user's step right/left motions ((a) JARoW displacement for the step left motion, (b) statistic data (cm))

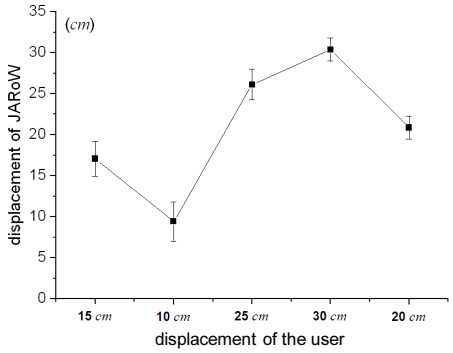

Fig. 12. JARoW displacement according to stride lengths

adapting to the user's behavior using a simple feedback control.

To examine JARoW's movement accuracy, the moving forward and step right/left motion were tested. As a subject took 100 steps of uniform length of 30 cm forward, JARoW followed the stride length as closely as possible as shown in Fig. 10. Figs. 10-(a) and (b) show the results by our previous control [11] and feedback control, respectively. Compared with Fig. 10-(a), the contour in Fig. 10-(b) became flattened, and the mean value and standard deviation were 30.26 and 1.66 cm, respectively. Similarly, in Fig. 11, JARoW followed the user's step right and left motions for 40 steps of uniform length of 20 cm. These results show that JARoW could generate the moving forward and step right/left motions corresponding to actual user stride lengths and stride rates. The moving forward behavior was re-tested with varying the stride length in the following order: 15, 10, 25, 30, and 20 cm. The statistical analysis results from 100 trials are presented in Fig. 12. The variation appeared most significant for the 10 cm stride, but the strides exceeding 20

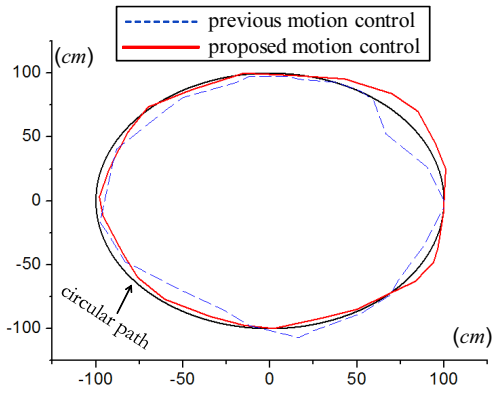

Fig. 13. Trajectory results of JARoW for following a circular path

Fig. 14. Forward movement of JARoW around a corner

cm showed relatively less fluctuations. It is also confirmed that the feedback control scheme is robust against faulty measurements in previous time steps.

Next, to investigate the validity of the feedback rotation control, the circular path following experiments were performed. A subject walks along the circular path with the radius of 1 m clockwise and counterclockwise as shown in In Fig. 13 The blue dotted line and red solid line indicate the JARoW trajectories with our previous control [11] and proposed feedback control, respectively. The proposed feedback control enabled JARoW to generate smooth turning right/left motions.

Finally, Fig. 14 shows snapshots for the forward and rotational movements around a corner in a hallway. It is observed that JARoW was controlled successfully in the indoor environment without experiencing any collision. JARoW is also expected to be used to assist visually impaired people. In contrast to existing active walkers, our walker features simple structure and compact size that can be fit into our everyday environment. More notably, the proposed feedback control allows users to easily control JARoW without requiring any mental or physical efforts.

VI. Conclusions

This paper presented an enhanced control method for JARoW that is easy to handle and transport. First, we proposed a natural user interface without requiring any user operations, through the use of a pair of LRFs. Secondly, the Kalman filter based user's lower limb location tracking scheme was developed to plan the motions of JARoW according to the user walking motions. Thirdly, the feedback control adjusted the motions of JARoW corresponding to the actual user walking behaviors. Fourthly, an obstacle avoidance scheme was implemented to achieve safe navigation in indoor environments. To demonstrate the effectiveness of the proposed control functions, different types of experiments were performed and the results were quite encouraging. As our future study, considering elderly people with poor posture who tend to lean their upper body onto the upper frame, a more sophisticated controller will be developed to cope with unpredictable changes in the JARoW dynamics.

References

[1] H. Ikeda, Y. Katsumata, M. Shoji, T. Takahashi, and E. Nakano, "Cooperative strategy for a wheelchair and a robot to climb and descend a step," *Advanced Robotics*, 22(13-14):1439-1460, 2008.

[2] C.-H. Kuo, H.-W. Yeh, and C.-E. Wu, "Development of autonomous navigation robotic wheelchairs using programmable system-on-chip based distributed computing architecture," *Proc. IEEE Int. Conf. Systems, Man and Cybernetics*, 2939-2944, 2007.

[3] H. Yu, M. Spenko, and S. Dubowsky, "An adaptive shared control system for an intelligent mobility aid for the elderly," *Autonomous Robotics*, 15(1):53-66, 2003.

[4] A. Veg and D. B. Popovic, "Walkaround: mobile balance support for therapy of walking," *IEEE Transactions on Neural Systems and Rehabilitation Engineering*, 16(3):264-269, 2008.

[5] Y. Hirata, A. Hara, and K. Kosuge, "Motion control of passive intelligent walker using servo brakes," *IEEE Transactions on Robotics*, 23(5):981-990, 2007.

[6] H. Kobayashi, T. Karato, and T. Tsuji, "Development of an active walker as a new orthosis," *Proc. IEEE Int. Conf. Mechatronics and Automation*, 186-191, 2007.

[7] K. Kong and D. Jeon, "Design and control of an exoskeleton for the elderly and patients," *IEEE/ASME Transactions on Mechatronics*, 11(4):428-432, 2006.

[8] V. Kulyukin, "Human-robot interaction through gesture-free spoken dialogue," *Autonomous Robots*, 16(3):239-257, 2004.

[9] H. Yano, Y. Hosomi, K. Aoki, R. Nanba, T. Hirotomi, and Satoru Okamoto, "Unstable motion detect system for four-casterd walker," *IEICE technical report, Speech*, 107(434):13-18, 2008.

[10] M. Hirasawa, H. Okada, and M. Shimojo "The development of the plantar pressure sensor shoes for gait analysis," *Journal of Robotics and Mechatronics*, 20(3):324-330, 2007.

[11] G. Lee, T. Ohnuma, and N. Y. Chong, "Design and control of JAIST active robotic walker," *Journal of Intelligent Service Robotics*, 3(3):125-135, 2010.

[12] J. M. Burnfield and C. M. Powers, "Normal and pathologic gait" in *Orthopaedic physical therapy secrets*, J. D. Placzek and D. A. Boyce (edt.), Hanley and Belfus (2nd ed.), 2006.

[13] P. S. Maybeck, *Stochastic models, estimation, and control*, Academic Press; 1982.

[14] T. Kirubarajan and Y. Bar-Shalom, "Probabilistic data association techniques for target tracking in clutter," *Proceedings of the IEEE*, 92(3):536-557, 2004.

[15] J. Borenstein and Y. Koren, "Real-time Obstacle Avoidance for Fast Mobile Robots," *IEEE Transactions on Systems, Man, and Cybernetics*, 19(5):1179-1187, 1989.